Supplementary Information for Optimized Spatial Correlations for Broadband Light Trapping Nanopatterns in High Efficiency Ultra-thin Film a-Si:H Solar Cells

Vivian E. Ferry,[1,2] Marc A. Verschuuren,[3] Claire van Lare,[1]
Ruud E. I. Schropp,[4] Harry A. Atwater,[2] and Albert Polman[1]

[1]*Center for Nanophotonics, FOM - Institute AMOLF, Science Park 104, 1098XG Amsterdam, The Netherlands*

[2]*Thomas J. Watson Laboratories of Applied Physics, California Institute of Technology, Pasadena, California 91125, USA*

[3]*Philips Research Laboratories, High Tech Campus 4, 5656 AE Eindhoven, The Netherlands*

[4]*Utrecht University, Debye Institute for Nanomaterials Science, Section Nanophotonics, P.O. Box 80, 000, 3508 TA Utrecht, The Netherlands*

I. GENERATION OF THE PSEUDO-RANDOM PATTERNS

Each pseudo-random pattern was first generated over a 100 μm x 100 μm area. The center points of the pattern were chosen randomly and assigned a diameter. For example, the "random, medium" pattern was generated assuming a diameter of 250 nm Ag nanoparticles. Center points were chosen with a minimum separation of the diameter of the particle, constraining the pattern so that the Ag particles do not overlap. Points were chosen until the number of valid points was equal to the number of points contained in the same area with a 400 nm pitch of particles. The "random, small" pattern assumed a diameter of 200 nm, and the "random, large" pattern of 300 nm. The array was then stitched together to form a 6 mm x 6 mm pattern, with care taken on the edges of the stitching boundary to ensure that the same non-overlapping conditions and packing fractions held. The "random, varying" pattern was generated using a mixture of the three different diameters, with each particle assigned a diameter before placement to check the overlap conditions.

II. TABLES OF BEST MEASURED JV DATA FOR EACH PATTERN

Each patterned region on the master substrate was 6 mm x 6 mm in area. After deposition of the a-Si:H layer, an array of 4 mm x 4 mm squares of ITO was sputtered through a contact mask, and finger contacts were evaporated over the ITO using a second contact mask. The cell active area used for determining J_{sc} (0.13 cm^2) is the area of the ITO contact (0.16 cm^2) less the area of the Au contact grid, and was verified by optical microscopy.

While several copies of each cell pattern were made, the best efficiency values are tabulated here in addition to the average values in parentheses. Where patterns are missing, all of the cells of that pattern on the substrate were shunted. An analysis of the growth statistics is beyond the scope of this paper.

III. EQE DATA FOR OTHER THICKNESSES AND REPEATABILITY

EQE measurements on the other thickness cells are shown in Supplementary Fig. 1. The 400 nm pitch cells in the 115 nm and 150 nm intrinsic layer thickness cells show blue side enhancement, the periodic cells show sharp features from the waveguide modes, and the pseudo-random patterns show a smooth response. Supplementary Fig. 1(c) shows

Thickness (nm)	Pattern	Eff.(%)	J_{sc} (mA/cm^2)	V_{oc} (V)	FF
90	400/Large	9.35 (*8.68*)	16.24 (*15.97*)	0.920 (*0.87*)	0.63 (*0.63*)
90	400/Medium	9.60 (*8.16*)	16.94 (*15.22*)	0.864 (*0.86*)	0.66 (*0.62*)
90	400/Small	8.87 (*8.27*)	16.10 (*15.75*)	0.865 (*0.85*)	0.64 (*0.61*)
90	500/Large	8.72 (*8.47*)	15.85 (*15.13*)	0.870 (*0.88*)	0.63 (*0.64*)
90	500/Medium	8.77 (*7.48*)	15.37 (*14.51*)	0.889 (*0.86*)	0.64 (*0.60*)
90	500/Small	8.66 (*7.65*)	14.60 (*13.30*)	0.897 (*0.88*)	0.66 (*0.65*)
90	Random/Large	9.44 (*8.09*)	16.84 (*14.41*)	0.872 (*0.86*)	0.64 (*0.65*)
90	Random/Medium	9.35 (*7.73*)	16.18 (*14.82*)	0.888 (*0.87*)	0.65 (*0.58*)
90	Random/Small	7.27 (*6.58*)	14.22 (*12.76*)	0.835 (*0.84*)	0.61 (*0.62*)
90	Random/Varying	8.88 (*8.21*)	16.68 (*15.62*)	0.855 (*0.86*)	0.62 (*0.61*)
90	Penrose	9.26 (*8.36*)	16.72 (*15.08*)	0.864 (*0.87*)	0.64 (*0.64*)
90	Flat	6.32 (*6.28*)	11.52 (*11.42*)	0.845 (*0.85*)	0.65 (*0.65*)
90	Asahi	6.94 (*6.69*)	12.52 (*12.93*)	0.890 (*0.83*)	0.62 (*0.62*)

TABLE I: JV measurements on cells with 90 nm intrinsic layer thickness

Thickness (nm)	Pattern	Eff.(%)	J_{sc} (mA/cm^2)	V_{oc} (V)	FF
115	400/Large	9.37 (*8.16*)	15.71 (*15.59*)	0.912 (*0.85*)	0.65 (*0.61*)
115	400/Small	5.91 (*5.72*)	13.66 (*12.31*)	0.833 (*0.84*)	0.52 (*0.56*)
115	500/Large	7.54 (*6.82*)	14.31 (*13.56*)	0.862 (*0.82*)	0.61 (*0.61*)
115	500/Medium	5.88 (*5.82*)	12.92 (*12.58*)	0.789 (*0.78*)	0.58 (*0.59*)
115	500/Small	5.75 (*5.63*)	12.26 (*12.42*)	0.782 (*0.77*)	0.60 (*0.57*)
115	Random/Large	7.49 (*6.53*)	14.93 (*13.93*)	0.834 (*0.79*)	0.60 (*0.59*)
115	Random/Medium	6.47 (*5.09*)	13.53 (*13.47*)	0.787 (*0.75*)	0.61 (*0.50*)
115	Random/Small	6.23 (*5.89*)	10.95 (*11.68*)	0.890 (*0.84*)	0.63 (*0.60*)
115	Random/Varying	8.06 (*7.29*)	15.90 (*14.25*)	0.832 (*0.84*)	0.61 (*0.61*)
115	Penrose	7.64 (*7.57*)	15.57 (*15.53*)	0.812 (*0.81*)	0.60 (*0.60*)
115	Flat	3.62 (*3.47*)	9.770 (*9.06*)	0.737 (*0.74*)	0.50 (*0.52*)

TABLE II: JV measurements on cells with 115 nm intrinsic layer thickness

Thickness (nm)	Pattern	Eff.(%)	J_{sc} (mA/cm^2)	V_{oc} (V)	FF
150	400/Large	7.38 (*7.16*)	14.94 (*14.88*)	0.755 (*0.76*)	0.65 (*0.63*)
150	400/Medium	9.48 (*7.76*)	16.57 (*15.81*)	0.854 (*0.79*)	0.67 (*0.61*)
150	400/Small	8.26 (*7.28*)	15.54 (*14.66*)	0.818 (*0.80*)	0.65 (*0.62*)
150	500/Large	8.44 (*7.66*)	15.54 (*15.48*)	0.829 (*0.80*)	0.66 (*0.62*)
150	500/Medium	7.99 (*7.52*)	16.22 (*15.72*)	0.797 (*0.79*)	0.62 (*0.60*)
150	500/Small	6.55 (*6.27*)	13.95 (*13.75*)	0.733 (*0.74*)	0.64 (*0.61*)
150	Random/Large	8.17 (*7.94*)	16.53 (*16.08*)	0.797 (*0.80*)	0.62 (*0.62*)
150	Random/Medium	7.42 (*6.46*)	15.99 (*14.57*)	0.787 (*0.76*)	0.59 (*0.59*)
150	Random/Small	6.90 (*6.54*)	14.68 (*13.68*)	0.764 (*0.76*)	0.61 (*0.63*)
150	Random/Varying	8.02 (*6.65*)	15.47 (*14.48*)	0.809 (*0.77*)	0.64 (*0.59*)
150	Penrose	7.44 (*6.76*)	15.69 (*14.95*)	0.783 (*0.74*)	0.60 (*0.61*)
150	Asahi	7.61(*7.43*)	14.13 (*13.96*)	0.808 (*0.81*)	0.67 (*0.66*)

TABLE III: JV measurements on cells with 150 nm intrinsic layer thickness

the average EQE for the same pattern (400 nm pitch with large particles) on the three different thicknesses. The close overlap on the blue side of the spectrum indicate that the absorption here is independent of thickness (and limited by collection and parasitic ITO absorption). This is consistent with attributing blue side photocurrent enhancements to the top nanostructures.

Supplementary Fig. 2 shows the repeatability of the EQE data for different cells on the 115 nm thick cell substrate. Each trace is a different cell, and the colors match to different patterns. The peaks on the red side of the spectrum are clearly correlated with pitch, and the variations between cell measurements are small.

IV. ANALYSIS OF THE PENROSE PATTERN

EQE measurements for the penrose pattern are shown in Supplementary Fig. 3, with the simulated points overlaid. The penrose tiling is not periodic, but has long-range order. The particles are the same size as the medium nanoparticles. The EQE spectrum appears to be an intermediate case between the periodic arrays and the pseudo-random arrays, with a few

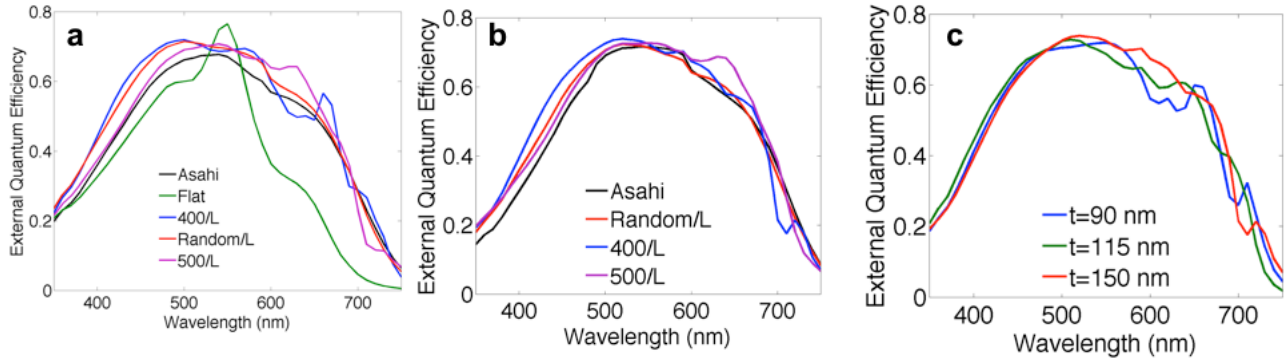

FIG. 1: EQE data on representative cells from other deposition runs. (a) 115 nm intrinsic regions. (b) 150 nm intrinsic regions. (c) 400 nm pitch nanopatterns with medium particles from each deposition run.

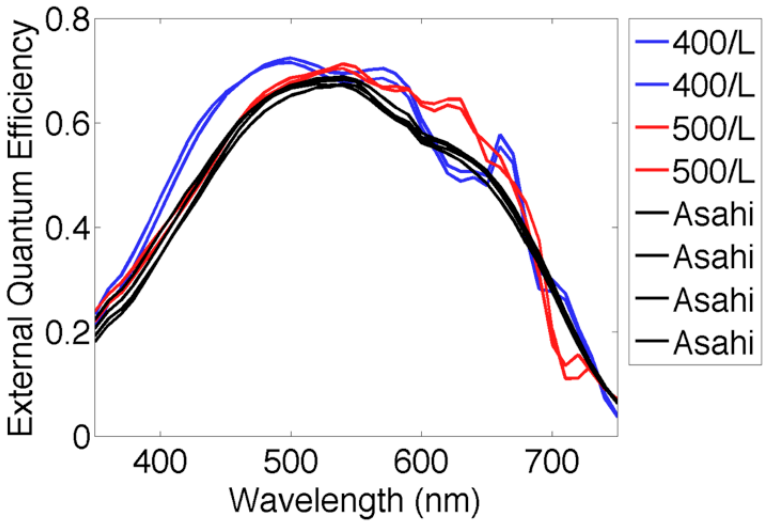

FIG. 2: Repeatability of EQE data on cells with 115 nm thick intrinsic regions. Each color trace is a different device on the substrate.

(repeatable) shoulders in the spectrum but much broader response than the periodic cells.

Supplementary Fig. 4 shows the PSD spectrum for the penrose pattern, generated from the AFM data, compared to a few of the other patterns. The penrose cell has higher PSD than the Asahi pattern, is comparable to the random, medium pattern, and is lower than the random, large pattern. Notably, the pattern shows reduced PSD in the undesirable low frequency range. Unlike the other patterns discussed, the penrose pattern does not have the

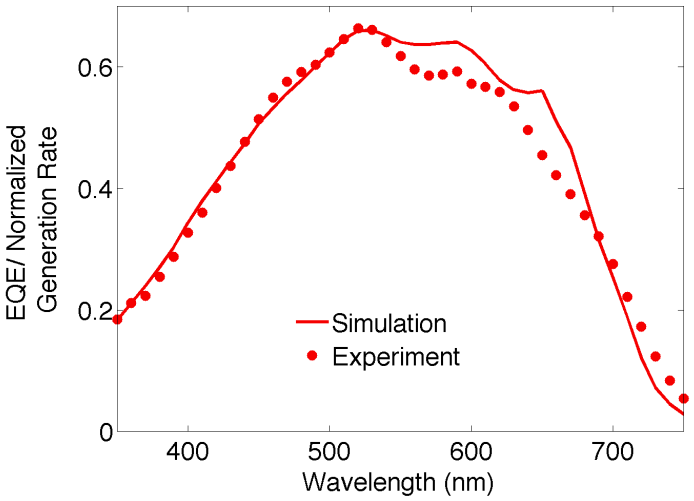

FIG. 3: EQE spectrum for penrose cell on 90 nm substrate, with overlaid simulation.

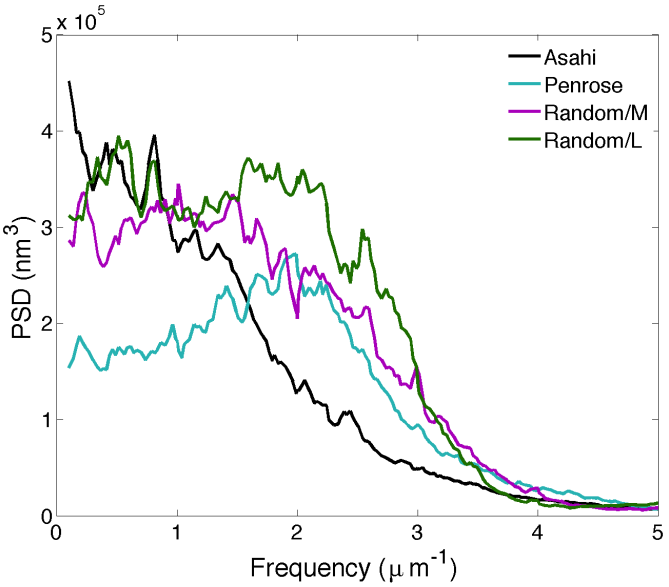

FIG. 4: PSD spectrum for penrose pattern compared to other pseudo-random patterns.

same packing fraction; the scatterers are less dense than the pseudo-random or 400 nm pitch patterns. For the pseudo-random patterns, modification of the diameter and pitch resulted in a significantly higher PSD. Given this, we expect the PSD for the penrose patterns could be tuned by modifying the diameter and spacing between the scatterers.

V. DETAILS OF SIMULATION LAYOUT

Electromagnetic simulations were performed using Lumerical Finite Difference Time Domain software, with home written post-processing code. The refractive index of each layer was taken from ellipsometric measurements, with Ag modeled by a Lorentz-Drude model. The simulations are performed at single wavelengths across the solar spectrum, and an index monitor map is used to separately calculate absorption in each of the layers, with only absorption in the a-Si:H contributing to the overall photocurrent. The simulations of Asahi texture were performed by feeding measured AFM data directly into the simulation, with a sufficiently large area to minimize boundary effects from the periodic edges. Simulations of the periodically nanopatterned cells assumed periodic boundary conditions, and approximated the aspect ratios and structures measured from cross sections. Simulations of pseudo-random patterns assumed the overcoating parameters of the periodic cells, with the simulation size of the Asahi textures.